Agricultural Water Management 273 (2022) 107907

Contents lists available at ScienceDirect

Agricultural Water Management

journal homepage: www.elsevier.com/locate/agwat

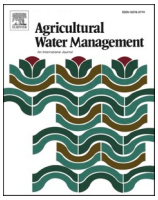

Rice ponding date detection in Australia using Sentinel-2 and Planet Fusion imagery

James Brinkhoff [a,*], Rasmus Houborg [b], Brian W. Dunn [c]

[a] University of New England, Armidale, NSW 2351, Australia
[b] Planet Labs Inc., San Francisco, CA 94107, USA
[c] NSW Department of Primary Industries, Yanco, NSW 2703, Australia

ARTICLE INFO

Handling Editor - J.E. Fernández

Keywords:
Rice
Irrigation management
Remote sensing
Time-series
Logistic regression

ABSTRACT

Rice is unique, in that yields are maximized when it is grown under ponded (or flooded) conditions. This however has implications for water use (an important consideration in water-scarce environments) and greenhouse gas emissions. This work aimed to provide precise predictions of the date when irrigated rice fields were ponded, on a per-field basis. Models were developed using Sentinel-2 data (with the advantage of inclusion of water-sensitive shortwave infrared bands) and Planet Fusion data (which provides daily, temporally consistent, cross-calibrated, gap-free data). Models were trained with data from both commercial farms and research sites in New South Wales, Australia, and over four growing seasons (harvest in 2018–2021). Predictions were tested on the 2022 harvest season, which included a variety of sowing and water management strategies. A time-series method was developed to provide models with features including satellite observations from before and after the date being classified (as ponded or non-ponded). Logistic regression models using time-series features produced mean absolute errors for ponding date prediction of 4.9 days using Sentinel-2 data, and 4.3 days using Planet Fusion data. The temporal frequency of the Planet Fusion data compensated for the lack of spectral bands relative to Sentinel-2.

1. Introduction

Globally, rice is one of the most important staple food crops, and around 75 % of production is from irrigated environments (Chauhan et al., 2017). Yields are optimized when rice is grown in ponded (flooded) conditions (Bouman et al., 2007). However, water scarcity is an increasing pressure on rice production, which has motivated research on optimizing the trade-off between yield and water use. Non-ponded growing systems include aerobic (Nie et al., 2012), and alternate wetting and drying (AWD) (Carrijo et al., 2017). Rice water management strategies also impact ecology and birdlife (Herring et al., 2021; Ranghetti and Boschetti, 2022) and greenhouse gas emissions (Linquist et al., 2015). These factors drive demand for systems that can determine rice water management across growing regions, and track changes in farmer practices over time (Ranghetti and Boschetti, 2022).

Ponding for at least some of the growing season remains the dominant practice due to improved yields and other agronomic factors such as weed control (Bouman et al., 2007). Ponding, however, incurs a penalty on water use due to non-productive water loss from soil drainage and evaporation. Soil drainage may be ameliorated through using only fields with non-leaky soils and puddling (Humphreys et al., 2006). Evaporation can be reduced by minimizing the duration of ponding, particularly during the early growth stages when canopy coverage is not complete (and thus evaporative losses are higher). Some hybrid systems seek to minimize the ponding period, restricting it to critical growth phases Bouman and Tuong (2001). In Australia, the delayed permanent water (DPW) system involves drill sowing rice into dry soil, after which a number of flush irrigations are applied during early growth stages to meet crop water demand. Rice fields are flooded before the microspore growth stage, which is particularly important in temperate growing regions as the water provides a temprature buffer to reduce yield penalties due to cold-induced sterility (Dunn and Gaydon, 2011). Rice water management also affects phenology, with growth accelerating after ponding. Tools that predict rice growth stage are significantly more accurate when the underlying models factor in not only planting date, but also ponding date (Darbyshire et al., 2019).

These factors motivate the development of industry-wide monitoring systems that can accurately determine per-field water application dates.

* Corresponding author.
E-mail address: james.brinkhoff@une.edu.au (J. Brinkhoff).

https://doi.org/10.1016/j.agwat.2022.107907
Received 16 March 2022; Received in revised form 1 August 2022; Accepted 22 August 2022

Such systems will facilitate assessment of the adoption of water-saving practice (such as delayed ponding) and will improve accuracy of growth stage prediction tools. Remote sensing provides data at the scale and frequency necessary for the development of such systems (Busetto et al., 2017; Nelson et al., 2014; Ranghetti and Boschetti, 2022).

Synthetic aperture radar (SAR) data has shown promise for mapping rice area (Torbick et al., 2017) and phenology (Inoue et al., 2014). One of the key advantages of SAR data are its low sensitivity to cloud cover, making it particularly crucial for use in frequently cloudy regions such as the tropics. Some work (Thorp and Drajat, 2021) has fused SAR with optical data, which slightly improved classification of phenology over using optical data alone, which in turn provided better results than using SAR data alone. Guo et al. (2019) similarly combined SAR and optical data to map rice in Australia, particularly focusing on ameliorating the challenge of reduced water signature when ponding is only applied after significant canopy coverage has been achieved. However, Sentinel-1 revisit over much of the rice growing area of New South Wales, Australia, is 12 days, which is not sufficient for accurately determining the precise date of ponding.

Rice field monitoring products based on optical satellite data have also been developed (Boschetti et al., 2017; Ranghetti et al., 2018). MODIS data are daily, but at very limited resolution of 250-m (red and near-infrared only) or 500-m. Landsat has 30 m resolution, and an archive of more than 30 years, with 16 day revisit (or 8 days with two satellites). The recent Sentinel-2 satellites provide 10, 20 or 60 m resolution (depending on band), and revisit from 3 to 7 days (Li and Roy, 2017). These all provide the shortwave infrared (SWIR) bands, which are sensitive to water (Brinkhoff et al., 2022), important for rice because of the ponded environment (Boschetti et al., 2014).

A recent development is near-daily imagery at 3 m resolution, such as from the Planet Dove cubesat constellation. This data source does have limitations, particularly the lack of SWIR bands, and challenges associated with cross-calibration between the many ($>$ 150) sensors in orbit. Planet Fusion (Planet Fusion Team, 2021) constitutes a comprehensive harmonization and fusion methodology based on the cubesat enabled spatio-temporal enhancement method (CESTEM) (Houborg and McCabe, 2018a), which effectively resolves cross-calibration and sensor interoperability issues by calibrating the cubesat sensors against a deep stack of Sentinel-2 and Landsat 8 surface reflectance imagery, whilst simultaneously filling gaps due to cloud and missing observations, thus providing a daily calibrated dataset.

Much previous work has been devoted to rice field mapping (Torbick et al., 2017; Guo et al., 2019; Niel and McVicar, 2003; Stroppiana et al., 2019). These exploit the distinctive water features of rice crops to distinguish them from other crops. Whilst some of these provide coarse estimates of ponding or start-of-season (Xiao et al., 2022), few studies have attempted to determine the precise dates that ponded water was applied, which requires field-level observations across regions and years to train models. Accurate ponding date predictions are needed for phenology prediction tools (Darbyshire et al., 2019), water use assessments (Qiu et al., 2021) and water management practice monitoring through time.

We aim to develop a methodology to detect the date of ponding of rice fields across an entire growing region, where a diverse range of water management practices are adopted (aerial and dry broadcast sowing with early ponding, drill sowing with flush irrigations and various delays before ponding). We compare predictions using Sentinel-2 (S2) imagery (with its advantage of measuring reflectance in the SWIR wavelengths), to Planet Fusion (PF) imagery (with its advantages of high spatio-temporal consistency and daily image frequency). We compare simple reflectance threshold based models with machine learning models, and assess the error of ponding date prediction for each method. The developed methods will provide improved data to the rice industry, facilitating improved phenological predictions, and assessing the growth in adoption of water-saving practices.

2. Methods

2.1. Location and study sites

This study was based in the irrigated rice growing regions of New South Wales, Australia (Fig. 1, showing irrigation areas obtained from Australian Bureau of Agriculture and Resource Economics and Sciences, 2022). The climate is temperate, allowing production of one crop per year. Crops are sown in late spring (typically October), flowering occurs in mid-summer (January), and harvest is in Autumn (April or May). There are a variety of sowing and water management practices adopted in the area (Ward et al., 2021), which are illustrated in Fig. 2. Traditional methods include dry broadcast (DB, where fields are ponded soon after seed distribution) and aerial sowing (ponding immediately before spreading pre-germinated seed into the water). Recently, drill sowing has been widely adopted because of its water saving benefits. Seed is drilled into dry soil, then a number of intermittent irrigations are applied before ponding at around the three-leaf vegetative growth stage (Dunn and Gaydon, 2011), typically late November. Delayed permanent water (DPW) (Dunn and Gaydon, 2011) further delays ponding until late December, just before the panicle initiation growth phase. Water management strategies that eliminate a period of continuous ponding altogether, such as alternate wetting and drying (Carrijo et al., 2017), are not standard practice in the study area (Dunn et al., 2014). Fields are drained around physiological maturity, late-March or early-April, and dried for harvest (Ward et al., 2021).

The study locations included 182 fields, and five harvest years 2018–2022 (Fig. 3). Note that throughout this paper, "year" refers to the year of harvest rather than the planting year (planting in Australia occurs the year before harvest, i.e. planting in October, harvest in April). We define day of season (DOS) as the days since 1-July of the year prior to harvest (corresponding approximately to day of year in the northern hemisphere). The fields were distributed across a commercial site used for research and seed production, two field research stations and numerous commercial farms (Fig. 1). For each field, the ponding date was recorded.

2019 and 2020 were drought years (Australian Government Bureau of Meteorology, 2019), resulting in much less rice grown overall (Australian Bureau of Statistics, 2020), and so less field observations were available in those years (Fig. 3). The study period thus includes dry and wet seasons, reflective of the variability in water availability typical of the system.

We used 2018–2021 data for training, then tested models on the 2022 data. Unfortunately, there were no DB/aerial sown crops within the smaller Planet Fusion tiles used in 2018–2021 (Fig. 1), explaining the lack of early ponding data points for those years (Fig. 3), different to the 2022 test dataset where a variety of sowing methods are used within the larger tiles. This presents a difficulty because, as shown in Fig. 2, drill sown crops have significant biomass by the time ponding is applied, in contrast to DB/aerial where the water signature is dominant at ponding. Therefore, it would be unreasonable to expect models trained on only drill-sown crops to be able to predict ponding dates of fields using other sowing methods. To solve this issue, we synthesized training data to mimic DB/aerial sowing, by including samples of an on-farm dam in the 2018–2021 dataset. The dam was within the study area (34°36′32"S 146°21′34"E), and had low NDVI and SWIR throughout the study period, similar to recently ponded aerial/DB crops. We labelled the dam samples as constantly ponded. The dam data points were duplicated to equalize the number of (synthetic) DB/aerial versus drill sown sites in the training data set. We note this method has limitations, as water applied to rice fields will have a range of spectral signatures depending on dissolved and particulate matter, water depth and substrate type (Fisher et al., 2016).

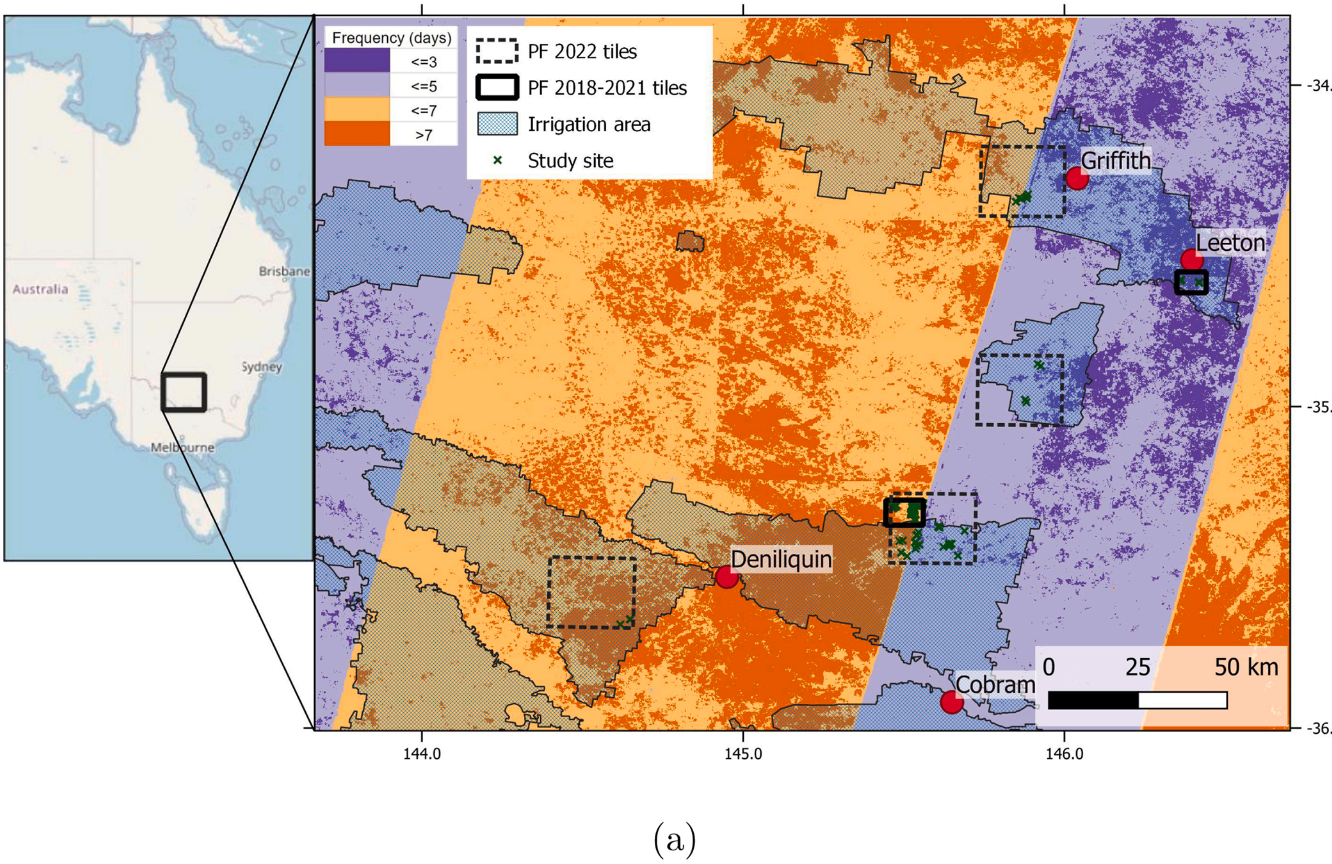

Fig. 1. Map of study fields and irrigation areas. The location of the Planet Fusion (PF) tiles are indicated (2 small tiles for 2018–2021 seasons in solid lines, 4 large tiles for 2022 in dashed lines). The background displays the average number of days between cloud-masked Sentinel-2 (S2) observations in 2022 (between 12 October and 15 January, or day of season (DOS) between 103 and 198, the range of ponding dates in the dataset).

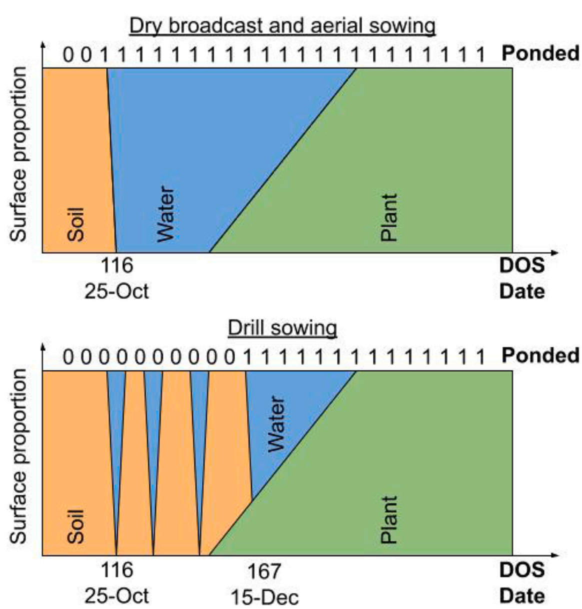

Fig. 2. Schematic of surface cover for individual paddocks, illustrating the main rice sowing methods used in the study area. The sowing date in both cases is 25-Oct. The ponded class is shown at the top of the diagrams, where 0 indicates dates before continuous ponding, and 1 after ponding. The date where the ponded class flips from 0 to 1 is the ponding date (25-Oct for dry broadcast or aerial sowing and 15-Dec for drill sowing).

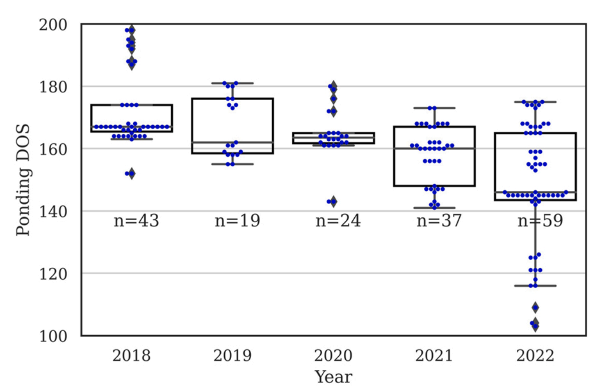

Fig. 3. Number of fields studied (n) per harvest year, totaling 182. The y-axis indicates the ponding day of season (DOS).

2.2. Remote sensing data

The remote sensing imagery was processed in the Google Earth Engine (GEE) platform (Gorelick et al., 2017). The study used two image sources, Sentinel-2 (S2) and Planet Fusion (PF), with characteristics shown in Table 1.

Four vegetation indices (VIs) were computed from the reflectances: .

- Normalized Difference Vegetation Index, NDVI = ND(NIR,R)
- Green Normalized Difference Index, GNDVI = ND(NIR,G)
- Green Red Vegetation Index, GRVI = ND(G,R)

Table 1
Sentinel-2 and Planet Fusion image characteristics. Revisit is the median across all study fields (after applying cloud masking for S2, see Section 2.2.1).

Band Name	S2 Center wavelength [μm]	PF (Resolution [m])
B	490 (10)	480 (3)
G	560 (10)	560 (3)
R	665 (10)	655 (3)
RE1	705 (20)	
RE2	740 (20)	
RE3	780 (20)	
NIR	835 (10)	865 (3)
NIR2	865 (20)	
SWIR1	1610 (20)	
SWIR2	2200 (20)	
Revisit	8.8 days	1 day

- Land Surface Water Index, LSWI = ND(NIR,SWIR1) (also known as NDWI)ND is the normalized difference operator:

$$ND(b1, b2) = \frac{b1 - b2}{b1 + b2} \quad (1)$$

These include all ND combinations of the G, R, and NIR bands. LSWI is frequently used in rice remote sensing because of its sensitivity to both open water and vegetation water content, but could only be derived from the S2 data because it requires a SWIR band Gao (1996)).

Models were developed using five combinations of reflectance bands and VIs, to assess which gave the best performance: .

- 4R = [B,G,R,NIR]
- 6R = [B,G,R,NIR,SWIR1,SWIR2] *
- 10R = [B,G,R,RE1,RE2,RE3,NIR,NIR2,SWIR1,SWIR2] *
- 3VI = [GRVI,GNDVI,NDVI]
- 4VI = [GRVI,GNDVI,NDVI,LSWI] *

Those marked * were specific to Sentinel-2 data due to reliance on SWIR and RE bands.

2.2.1. Sentinel-2

Sentinel-2 (S2) data are available in GEE, including both the top-of-atmosphere (L1C) and surface reflectance (L2A) collections. However the L2A collection in GEE does not extend back to 2017 (the year of planting for the 2018 harvest), so we used the L1C collection. Other work has used L1C data for the same reason, obtaining good results (Ni et al., 2021; Wolters et al., 2021).

Two levels of cloud amelioration were used. Firstly, tiles were filtered by the "cloudy pixel percentage" (CPP) metadata field. Secondly, at the pixel level, clouds are masked using the s2cloudless layer with a threshold of 40 % (Skakun et al., 2022), which is available in GEE. Cloud and shadow masking remains a challenging task, particularly for Sentinel-2, where the lack of thermal band can cause confusion over bright targets (Skakun et al., 2022), and shadows can be mistaken for water. We defined an "unmasked" parameter: .

- 0 when the cloud masking is ignored,
- 1 when > 99 % of pixels within each field for each image was unmasked,
- 2 when > 99 % of pixels within a radius of 500 m were unmasked,
- 3 when > 99 % of pixels within a radius of 2000 m were unmasked.

Settings 2 and 3 help reduce the impact of cloud shadows and cloud that wasn't successfully masked. There is a trade-off between image quality (better for more stringent filtering) and the number of images available for training and predicting (higher for less filtering). We tested prediction accuracy versus CPP, and with unmasked settings of [0,1,2,3]. After these two levels of cloud filtering, the number of days between images over each field varies, depending on seasonal cloud conditions and S2 tile overlaps (Fig. 1). For example, with CPP < 90, and unmasked= 2, the median days between images per field ranged between 3.7 and 11.7 days (median 8.8 days).

2.2.2. Planet Fusion

Planet Fusion (PF) data over 2 small tiles for 2018–2021 sites, and 4 larger tiles for 2022 sites (Fig. 1) were provided by Planet Labs. PF constitutes a comprehensive radiometric and geometric harmonization and fusion methodology based on the CESTEM algorithm (Houborg and McCabe, 2018a,b). PF performs multi-sensor inter-calibration and data fusion leveraging rigorously calibrated and freely available datasets from Sentinel-2, Landsat 8, Moderate Resolution Imaging Spectroradiometer (MODIS), and Visible Infrared Imaging Radiometer Suite (VIIRS) in concert with the higher spatial and temporal resolution CubeSat images from the PlanetScope Constellations. PF uses the Framework for Operational Radiometric Correction for Environmental Monitoring (Frantz, 2019) to generate a 30 m harmonized Sentinel-2 and Landsat 8 BRDF adjusted surface reflectance (SR) product to be used as the calibration target during the CESTEM-based radiometric harmonization step. Additional PF features include 1) sub-pixel geometric alignment of source imagery, 2) rigorous, temporally driven, cloud and cloud shadow detection, 3) fusion of Sentinel-2 and Landsat 8 data to help fill gaps in PlanetScope coverage, and 4) advanced gap-filling (Planet Fusion Team, 2021). PF delivers daily, gap-filled, 4-band (0.45–0.51, 0.53–0.59, 0.64–0.67, 0.85–0.88 μm) sensor agnostic SR data characterized by enhanced radiometric stability and consistency across space and time domains.

The data included daily imagery from 1 September 2017 to 31 May 2022. Data were ingested and processed in GEE. Because of the aforementioned Planet Fusion characteristics, no pre-processing apart from computation of vegetation indices (GNDVI, NDVI and GRVI) was necessary.

2.3. Data engineering and classification

The spatial mean per field × image-date, of all reflectance bands and vegetation indices was computed for the S2 and PF image collections. This resulted in a time-series table with all combinations of image date and field as rows, and reflectance and VI statistics as columns.

The aim is to predict the date of ponding, for which there are numerous possibilities of organizing data to train and assess models. We chose a method that classifies each image date of each field as either pre-ponding (Ponded=0) or post-ponding (Ponded = 1). This is then a binary classification problem, with a long dataset (rows = number of fields × images per field). A small period of the data for one field from the 2019 harvest year is shown in Table 2a.

If only one date of image data is available for classifying each row, ponding could be confused with the presence of intermittent water, such as from pre-ponding irrigation or rainfall, as found by Xiao et al. (2022). Therefore, we adopted a time-series approach that transforms the table, so that each row allows the model to see a specified number of previous (pre) and future (post) images (Table 2b). The total number of features available to a classifier is (pre+post+1) × nf, where nf is the number of base features before transformation (e.g. nf=4 when [B,G,R,NIR] are used). A range of pre and post values were trialed for the S2 and PF models. The model was applied to predicting the ponded class across the time series for all fields in the test data tables. Finally, the predicted ponding date for each field was extracted. Since PF provided daily data, the ponding date was the first date where the ponded class flips from 0 to 1. For S2, there are time gaps between images, leading to uncertainty in the precise date when the change occurred. We took the ponding date to be the mid-point between the first date where the ponded class became 1, and the date of the previous image (which had ponded class 0).

Once these data engineering steps were performed, the data was filtered to contain only DOS from 80 to 220 (a buffer of 22 days before

Table 2
(a) Example slice of one field's S2 data table, showing only the SWIR2 column. (b) Transformed data table ready for machine learning to predict the ponding class, using the SWIR2 predictor, with pre= 2 and post= 1 (for example, in (b), "− 1″ indicates data from the previous image and "+1″ indicates data from the subsequent image).

Date	DOS	SWIR2	Ponded
2018-12-12	164	0.167	0
2018-12-17	169	0.104	0
2018-12-22	174	0.041	1
2018-12-27	179	0.045	1

(a)

DOS	SWIR2-2	SWIR2-1	SWIR2+0	SWIR2+1	Ponded
164	0.265	0.227	0.167	0.104	0
169	0.227	0.167	0.104	0.041	0
174	0.167	0.104	0.041	0.045	1
179	0.104	0.041	0.045	0.071	1

(b)

and after the range of ponding dates in the dataset).

2.4. Model training and assessment

To ensure robust validation of models at predicting new years with no field observations, training and test data was separated by year. Test data was from the 2022 harvest year (planted in 2021), and training data from the previous four harvest years 2018–2021 (planted in 2017–2020).

We first assessed a simple threshold-based model using S2 data. The SWIR reflectances drop immediately after ponding and stays low after vegetation emerges, which has also been exploited in characterization of wetland inundation (Brinkhoff et al., 2022). The SWIR threshold was selected by varying it from 0.05 to 0.25 in steps of 0.005, finding the most recent date when the reflectance dropped below the threshold, then setting the ponding date prediction as the mid-point between that date and the previous image date. For each threshold, the prediction RMSE of ponding date over all data was calculated, with the optimal threshold selected by that which gave low RMSE. This procedure was performed separately on each of the training years 2018–2021, allowing assessment of the consistency of the threshold over years. The chosen threshold was then used to test predictions on 2022 data.

Then, machine learning (ML) models were trained using the logistic classifier in scikit-learn (Pedregosa et al., 2011). The ridge, support vector machine (SVM) and random forest (RF) classifiers were also assessed, but no advantage was found over the logistic classifier, and the latter trained significantly faster. The tuning hyperparameters of the classifiers were optimized using leave-one-year-out cross-validation (LOYO-CV Brinkhoff et al., 2019), to help ensure model predictions can be generalized to new years. In the case of the logistic classifier, the tuning hyperparameter was C, and the optimal value was selected using GridSearchCV in scikit-learn from a range of 0.001–10000.

Optimal data engineering settings (cloud filtering, pre and post images, feature set) were chosen by assessing the cross-validation balanced accuracy on the training data. The chosen settings were then applied to train a model on all training data (harvest years 2018–2021). The model was then tested on the data from the 2022 harvest year.

Test accuracy was assessed by comparing actual and predicted date of ponding. We computed the error as the difference between actual and predicted DOS of ponding. These errors were summarized using the root mean squared error (RMSE) and mean absolute error (MAE). RMSE accentuates large errors so is more sensitive to outliers, while MAE represents the average prediction performance. We also calculated Lin's Correlation Concordance (LCCC), which has a similar interpretation to the coefficient of determination (R^2), but is more useful for model prediction assessment, as it indicates how close to the 1:1 line the predicted vs actual values are, rather than simply how correlated they are (Lin, 1989).

3. Results

3.1. Time series characteristics

Examining the time-series evolution of reflectances and VIs provides intuition of how ponding can be detected (Fig 4). A dry broadcast or aerial-sown field has no vegetation when ponding starts, so NDVI becomes low or even negative (see negative NDVI at DOS = 118 in Fig. 4a, because NIR < R post ponding in Fig. 4b). In contrast, in drill sown fields (Fig. 4c), the rice plants have emerged by the time ponding occurs, so the remote sensor sees a mix of vegetation and water, thus NDVI is higher.

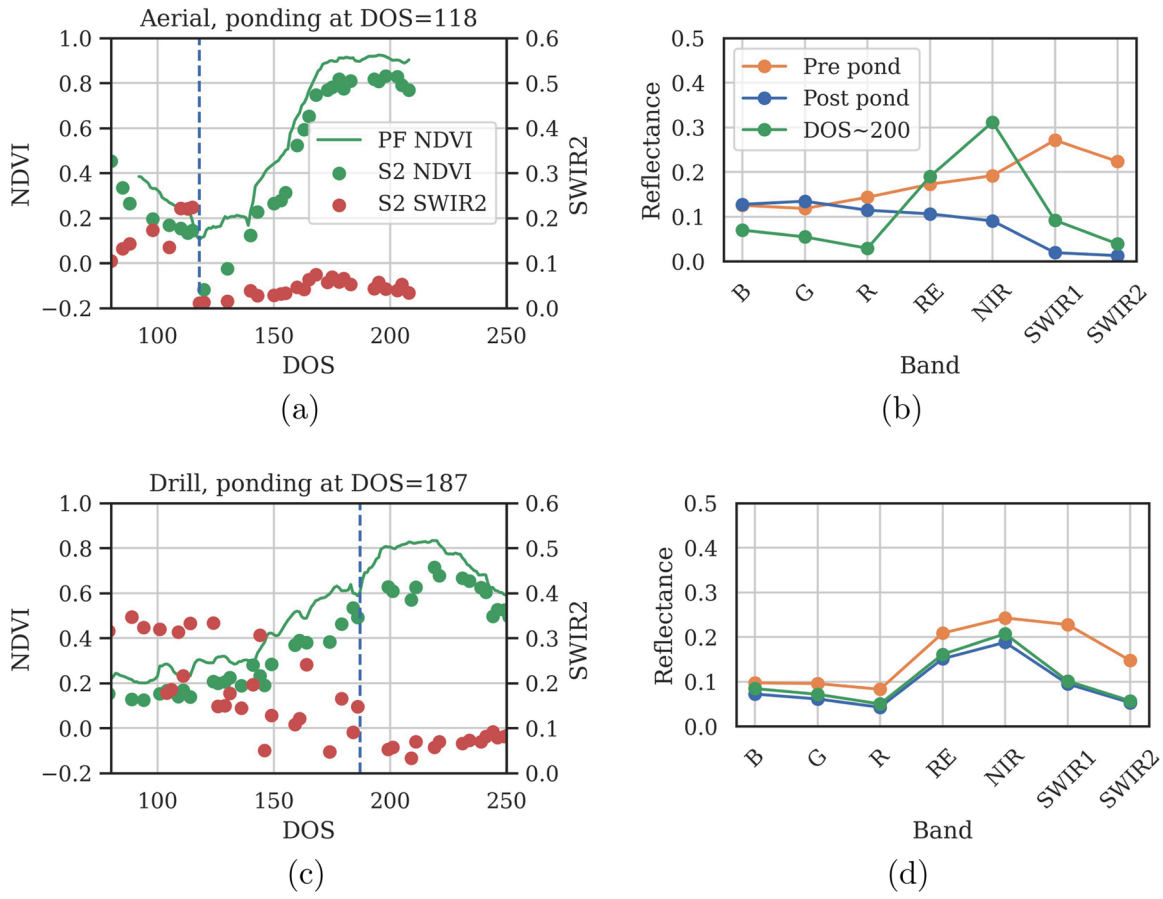

Fig. 4. Time series and reflectance plot of S2 (top-of-atmosphere L1C) and PF (surface reflectance) data for an (a–b) aerial sown, and (c–d) drill sown crop. The vertical blue line indicates the date of ponding. (For interpretation of the references to color in this figure legend, the reader is referred to the web version of this article.)

However, in both cases, the SWIR reflectances drop significantly following ponding, and remain low through vegetation growth. In contrast, NIR drops after ponding, but very quickly increases as the plants grow. The SWIR reflectances are thus a strong indicator of the presence of water (Brinkhoff et al., 2022).

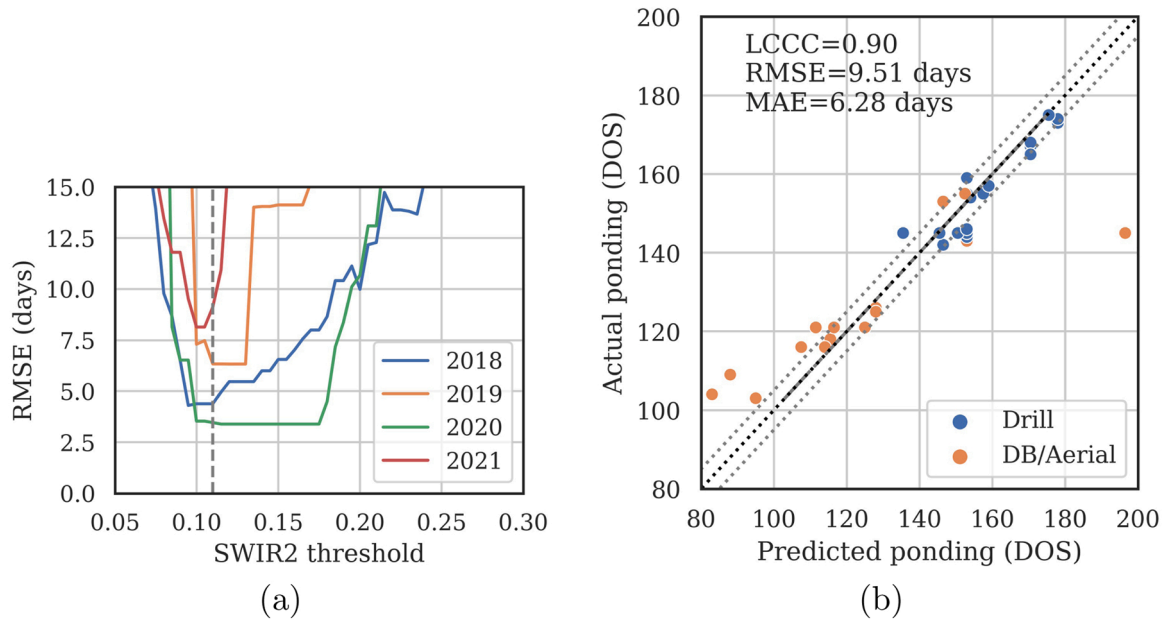

Fig. 5. (a) Optimal threshold for SWIR2 band per year. (b) Predicted vs actual ponding dates in 2022 using a threshold of SWIR2 = 0.11.

3.2. Threshold-based model

The threshold-based model searches for the latest date when the SWIR bands fall below a threshold, which is then used to determine the predicted ponding date. Best results were obtained with cloud filtering parameters CPP = 10 % and unmasked= 2. SWIR1 results were less consistent between years and had higher RMSEs compared with SWIR2. The SWIR2 optimal threshold was near 0.11 in all years (Fig. 5a).

Applying this model to 2022 test data resulted in an MAE of 6.3 days for ponding date prediction (Fig. 5b). 80 % of the predictions had errors less than 8 days. The biggest error (point with predicted ponding DOS=197 in Fig. 5b) was due to an anomalous spike in the SWIR2 reflectance over that field from an image acquired on DOS = 195 (2022–01–12), which was caused by cloud that was undetected by the cloud mask.

3.3. ML models

3.3.1. Sentinel-2

For the S2 ML models, an exhaustive search of five parameters was performed (900 combinations): (i) pre = [0,2,4], (ii) post = [0,2,4], (iii) cloud CPP= [10,30,50,70,90], (iv) unmasked= [0,1,2,3] and (v) 5 combinations of reflectances or VIs. We compared cross-validated (CV) leave-one-year-out balanced accuracy of classifying the ponding class among the combinations (training data only). We first examined the interaction between the cloud parameters CPP and unmasked (Fig. 6a). The best combination was CPP= 90 % (very little tile-based filtering), and unmasked= 2 (only retaining data with more than 99 % unmasked pixels within a radius of 500 m of the respective field image).

Then we held the cloud settings fixed at the above values, and examined the CV accuracy against pre and post images, and the feature sets (Fig. 6b–c). The SWIR bands are very important, as the worst results were obtained with feature sets that don't contain information from those bands (3VI and 4R). The highest accuracies were obtained using all reflectances (10R), which were slightly better than accuracies obtained using the vegetation indices including LSWI (4VI) and limited reflectance bands (6R). Results generally improved with the number of post images, and were less sensitive to the number of pre images. Our final parameter choice was CPP= 90, unmasked= 2, features= 10R, pre= 4 and post= 4, which gave a CV balanced accuracy score of 0.981. The total number of features for this model is (4 +4 +1) × 10 = 90, and there were 2066 rows for model training (not including duplicated dam samples).

These parameter settings were then used to train a model on all the 2018–2021 data, and ponding date predictions were tested by applying the model to the 2022 test data. The MAE was 4.9 days, with 80 % of the prediction errors less than 6.9 days (Fig. 7). Inspection of the time-series S2 data from the fields with the largest errors showed these had large gaps in the observations near the ponding date, due to cloud.

We tested predictions using S2 L2A surface reflectance data (instead of L1C top of atmosphere data). As noted in the Methods, there is less data available for this image collection. The prediction MAE degraded to 5.6 days (vs 4.9 days).

We had additional ponding data for fields that were outside the PF tiles (Fig. 1). These included DB/aerial sown fields in the training years (so the duplicated dam samples were not needed). This provided an

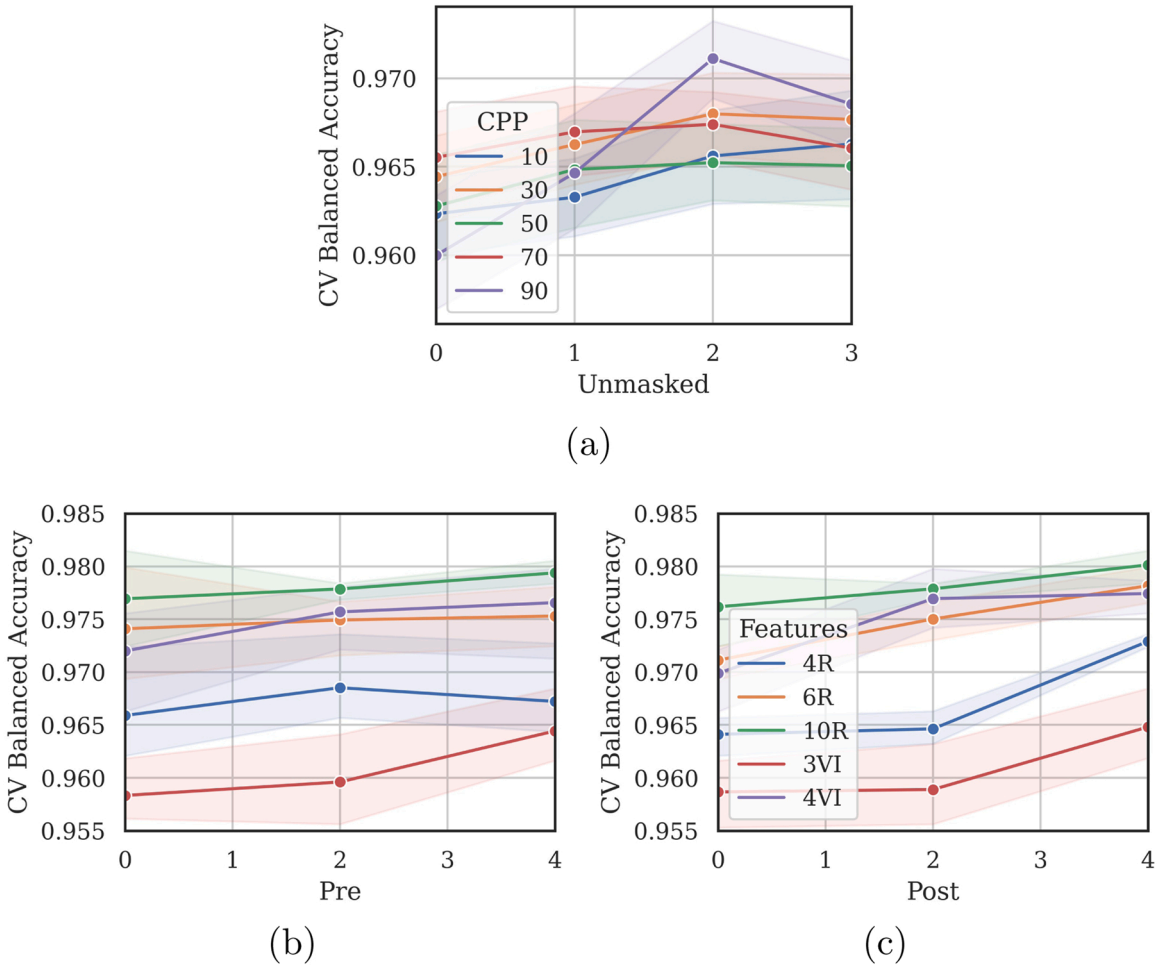

Fig. 6. S2 classifier optimum parameter search, showing the leave-one-year-out cross-validation balanced accuracy on the training data.

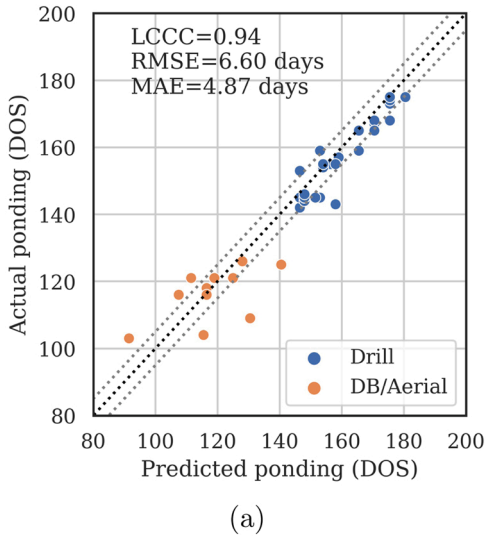

Fig. 7. Predicted vs actual ponding dates for the S2 ML model applied to the 2022 test data.

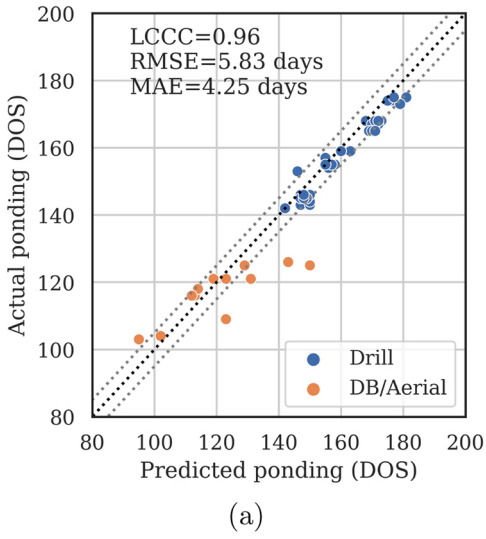

Fig. 9. Predicted vs actual ponding dates for PF ML model applied to the 2022 test data.

additional 9 training fields (2018–2021). The MAE reduced to 3.8 days (vs 4.9 days) with this additional data.

3.3.2. *Planet Fusion*

A similar parameter search was performed for models based on the PF data. The range in the 3 parameters were: (i) pre = [0,2,4,8,16], (ii) post = [0,2,4,8,16], and (iii) 4 reflectances vs 3 VIs. Based on cross-validated balanced accuracy on the training data, the best results were obtained with the 3VI feature set, which was significantly better than using the four reflectances (Fig. 8). The number of pre images had little impact, so we chose a value of 0. The results were best with 4 post images, with balanced accuracy of 0.972. The total number of features for this combination is $(4+1) \times 3 = 15$, and there were 17,220 rows for model training (not including duplicated dam samples).

The chosen parameters were used to train the final model, which was then tested using the 2022 data. For ponding date prediction, the overall MAE was 4.3 days (Fig. 9), and 80 % of the prediction errors (n = 59) were five days or less. The five worst predictions (errors from 8 to 25 days) were all DB/aerial-sown fields.

3.4. *Analysis of industry-wide water application dates*

We obtained a shapefile of the approximately 60,000 ha of rice fields planted in 2021, (harvested in 2022). The data included the sowing method (drill or aerial/DB) recorded by each farmer. The S2 time series was extracted for each field, and the optimal S2 ML model was used to predict the ponding date for each field. The results show the large variation in ponding dates across the industry (Fig. 10a). The DB/aerial fields generally have early ponding dates, whereas the drill fields have later ponding dates as expected. The distribution of ponding dates across the growing region shows the spread of grower water management practice (Fig 10b). Southern fields (close to half of the 2022 fields at latitude $< -35^{o}$) had earlier ponding dates (mean DOS=138) compared to northern fields (mean DOS=143). This corresponds to more fields being aerial/DB sown in the south than the north.

4. Discussion

We developed methods to predict rice ponding date, which are accurate for the variety of sowing methods and water management strategies adopted in Australia. Two image sources were assessed. Usable Sentinel-2 data had variable revisit due to cloud and tile overlap, with some fields having large time gaps leading to uncertainty in precise ponding date predictions. However, S2 had the advantage of measuring reflectance in the water-sensitive SWIR range. On the other hand, the Planet Fusion data had the advantage of daily revisit, providing much

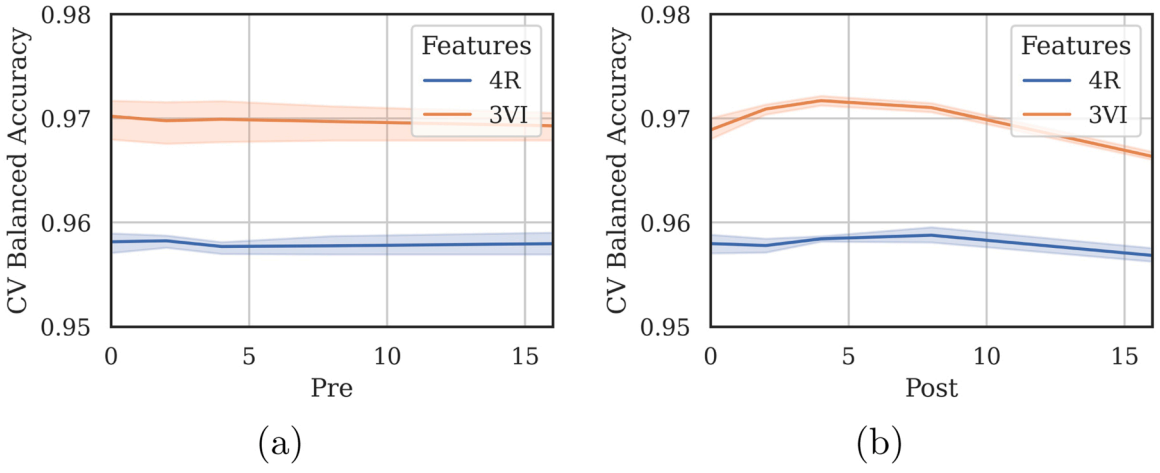

Fig. 8. Optimum PF classifier settings search, showing the leave-one-year-out cross-validation balanced accuracy on the training data.

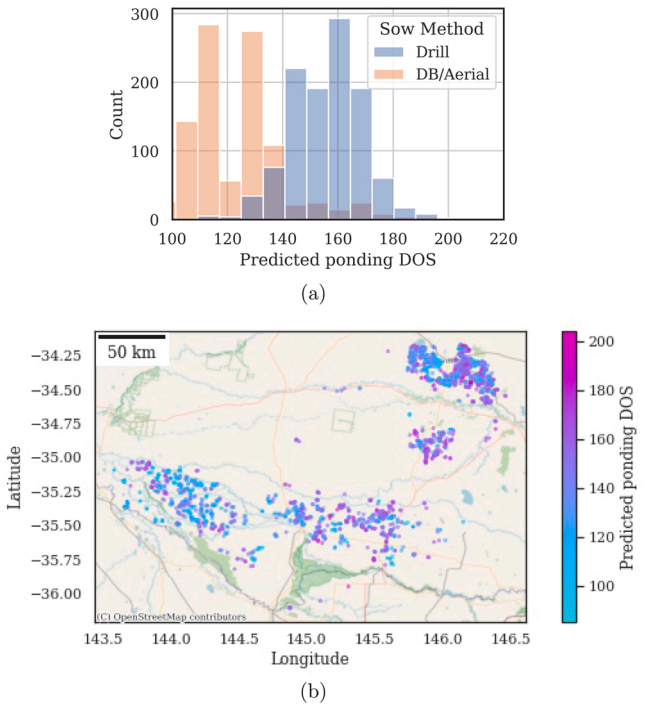

Fig. 10. Predicted ponding dates using the S2 ML model for approximately 60,000 ha of rice fields from the 2022 harvest season.

more training data points and no temporal gaps. A summary of results for the held-out test year of 2022 (Table 3) indicate average ponding prediction date errors less than 5 days are possible.

SWIR reflectance is a robust indicator of the presence of water, even when partially obscured by rice plants. Many previous rice studies have used SWIR-based indices such as LSWI to detect rice fields (Boschetti et al., 2014). For detecting water, indices involving SWIR reflectances are relatively insensitive to vegetation cover (Ji et al., 2009). However, as noted in studies of the inundation of wetlands with emergent vegetation (Wolski et al., 2017; Brinkhoff et al., 2022), using SWIR reflectances without resorting to derived indices can provide more accurate inundation predictions. Our simple threshold model indicates a S2-L1C SWIR2 threshold of 0.11 was optimal over years to identify rice field ponding. This method provided an easily interpretable model that could be implemented simply in geographic information systems. However, the ponding date predictions using this method were not as accurate as those produced by more complex ML methods, which could utilize a wider range of temporal and spectral features derived from the imagery.

A source of error for S2 models is cloud. In contrast to other works that apply fixed tile filtering thresholds and cloud masking (Ni et al., 2021), we included cloud filter parameters as part of the model optimization. We applied a pixel-based cloud mask, and tested accuracy when data was discarded that was partially masked over each field, and/or within the neighborhood (500 m and 2000 m radius) of each field. We also filtered the data by the S2 tile "cloudy pixel percentage" (CPP) metadata. There were variable gaps between consecutive images over the fields, with some fields having images at least every 4 days over a season, and others with gaps as large as 12 days. As ponding is a sudden event, temporal gaps reduce precision. Additionally, there was a tradeoff in the optimal setting for the cloud filtering. More stringent filtering retains only high quality images, but also provided less data for training models. On the other hand, more relaxed cloud filtering provided more data, but reduced overall image quality, including due to cloud shadows and clouds not detected by the masking algorithm. We found that using the pixel-based cloud masking, removing any data with masked pixels within 500 m of the respective field produced the most accurate predictive models.

Table 3
Summary of ponding date prediction errors for the 2022 test data (n = 59 fields).

	S2 Threshold	S2 ML	PF ML
MAE (days)	6.3	4.9	4.3
RMSE (days)	9.5	6.6	5.8
LCCC	0.90	0.94	0.96

We found that S2 L1C top of atmosphere data provided higher accuracy predictions than L2A surface reflectance data, which has been observed in other studies (Wolters et al., 2021). This may be at least partly be due to the incomplete L2A collection in GEE, making less data available for model training (Ni et al., 2021). We also found that using the raw reflectances, and particularly the SWIR bands, provided better accuracy than using derived vegetation indices.

The Planet Fusion dataset provides daily analysis-ready data, calibrated to Sentinel-2 surface reflectances. While it does not include SWIR bands, we found that ponding date prediction was more accurate using PF compared with S2 (MAE 4.3 vs 4.9 days). Our results show that for applications requiring detection of the precise timing of agronomic parameters, daily calibrated datasets such as PF are invaluable, with the high temporal frequency overcoming some of the limitations due to having less reflectance bands. This high frequency aspect has been similarly exploited in sowing date detection (Sadeh et al., 2019) and phenology prediction (Myers et al., 2019; Nieto et al., 2022).

As our method uses optical data, it is applicable to regions with limited cloud, which may not be the case in tropical regions. However, the data engineering and machine learning techniques proposed here could be applied SAR data to achieve similar outcomes. SAR data has been used in other studies to overcome the challenges related to cloud (Torbick et al., 2017; Stroppiana et al., 2019). Guo et al. (2019) fused Sentinel-1 SAR with Sentinel-2 multispectral data to map rice fields in one growing region in Australia, finding that this fusion increased classification accuracy significantly, particularly considering the range of delays between sowing and ponding. However, in our study area, the revisit of Sentinel-1 is 12 days, which is not sufficient for our particular application: predicting the actual date of ponding.

One limitation of our training data was that no dry-broadcast or aerial sown fields were available in the PF tiles. These have very different spectral signatures at ponding than drill sown fields. As unbalanced training data can lead to mis-classification of minority groups (Waldner et al., 2019), we synthesized training data approximating characteristics of the DB/aerial sowing methods at ponding by sampling reflectances of a permanent water body. We had additional DB/aerial data for training years outside the PF tiles. When we trained an S2 model using these, the MAE improved by 1.1 days, to 3.8 days. Therefore, with addition of increased training data from other sowing methods, we expect greater accuracies could be obtained with the PF models as well. Adopting additional data balancing methods, such as those described by Waldner et al. (2019) may further improve accuracy.

We used regularized logistic regression to classify each image date into pre-ponding or ponded. In the case of S2, using all 10 reflectance bands gave the best results. Generally, better results were obtained when more features were provided to the classifier. The SWIR features were particularly important, with the red-edge bands also providing some benefit. Reflectances were as good or better than vegetation indices for the S2 classifiers. For PF, less features are available, and the combination of three vegetation indices produced better results than four reflectances. We adopted a data transformation technique, allowing the classifier to use information from images before and after the date being classified. Access to data after the classification date was particularly valuable, probably avoiding the possibility of intermittent irrigations or rainfall being classified as ponding (as subsequent images would indicate that the surface dries again, which is not the case for ponding).

Providing industry-wide estimation of per-field ponding dates will

have many benefits for productivity and sustainability. Growers rely on accurate phenology dates, to guide decisions such as timing of fertilizer and water application (Dunn and Gaydon, 2011). This work will benefit models that predict growth stages of rice, such as panicle initiation, which are more accurate when the date of ponding is included as an input (Darbyshire et al., 2019). Industry-wide estimation of ponding dates will facilitate assessment of the adoption of water saving techniques, such as delayed permanent water (Dunn et al., 2014), and assessment of greenhouse gas emissions and impact on wildlife (Ranghetti and Boschetti, 2022). Combining ponding date predictions with yield data will enable provision of recommendations to growers to optimize the tradeoff between rice water use and productivity, decisions which are becoming increasingly important with increased demand for food production coupled with growing water insecurity.

5. Conclusion

Information on rice water application is important both for growers (to predict phenological stage, to manage inputs and assess impact of water saving irrigation techniques on productivity), and for industry and government (to track water use and greenhouse gas emissions). This work has demonstrated development of machine learning models, which use a time-series of optical imagery as predictors, to estimate the date of continuous ponding of rice fields across the main rice growing region of Australia. Including features from images acquired after the date being classified as ponded or non-ponded was particularly important. We compared models built using two imagery datasets. Models based on Sentinel-2 data were optimized when shortwave infrared bands were included. Planet Fusion does not include shortwave infrared bands, however, the daily frequency of this imagery resulted in more accurate ponding date predictions than the Sentinel-2 models. In both cases, the mean absolute error of ponding date predictions were less than 5 days.

Declaration of Competing Interest

The authors declare that they have no known competing financial interests or personal relationships that could have appeared to influence the work reported in this paper.

Data availability

The data that has been used is confidential.

Acknowledgements

The authors are grateful to Ben Heaslip of Rice Research Australia Pty Ltd (RRAPL) for field data. Additional field observations were gathered by Tina Dunn, Chris Hodges, Craig Dawes, Alex Schultz, Sam North, Don Griffin, Troy Mauger and Annabelle Arnold. Planet Labs provided the Fusion imagery. This work was funded by AgriFutures, grants PRO-013078 (Real-time remote-sensing based monitoring for the rice industry) and PRJ-009790 (Rice variety nitrogen and agronomic management). We are thankful for the work of the anonymous reviewers who provided many helpful suggestions.

References

Australian Bureau of Agriculture and Resource Economics and Sciences, Australian Irrigation Areas (Vector), Version 1A, National Land and Water Resources Audit. ⟨https://data.gov.au/data/dataset/australian-irrigation-areas-vector-version-1a-national-land-and-water-resources-audit⟩. (Accessed 28 July 2022).

Australian Bureau of Statistics 2020. Agricultural Commodities, Australia, 2018–19 financial year. ⟨https://www.abs.gov.au/statistics/industry/agriculture/agricultural-commodities-australia/2018–19⟩. (Accessed 28 July 2022).

Australian Government Bureau of Meteorology, 2019. Australian Water Outlook - 2019 Relative Precipitation.⟨https://awo.bom.gov.au/products/historical/precipitation/4.5,-27.509,134.221/nat,-31.588,147.066/r/y/2019⟩. (Accessed 28 July 2022).

Boschetti, M., Busetto, L., Manfron, G., Laborte, A., Asilo, S., Pazhanivelan, S., Nelson, A., 2017. PhenoRice: a method for automatic extraction of spatio-temporal information on rice crops using satellite data time series. Remote Sens. Environ. 194, 347–365. https://doi.org/10.1016/j.rse.2017.03.029.

Boschetti, M., Nutini, F., Manfron, G., Brivio, P.A., Nelson, A., 2014. Comparative analysis of normalised difference spectral indices derived from MODIS for detecting surface water in flooded rice cropping systems. PLoS One 9 (2), e88741. https://doi.org/10.1371/journal.pone.0088741.

Bouman, B., Humphreys, E., Tuong, T., Barker, R., 2007. Rice and water. In: In: Advances in Agronomy. Elsevier, pp. 187–237 volume 92, pp.

Bouman, B.A.M., Tuong, T.P., 2001. Field water management to save water and increase its productivity in irrigated lowland rice. Agric. Water Manag. 49, 11–30. https://doi.org/10.1016/S0378-3774(00)00128-1.

Brinkhoff, J., Backhouse, G., Saunders, M.E., Bower, D.S., Hunter, J.T., 2022. Remote sensing to characterize inundation and vegetation dynamics of upland lagoons. Ecosphere 13, e3906. https://doi.org/10.1002/ecs2.3906.

Brinkhoff, J., Dunn, B.W., Robson, A.J., Dunn, T.S., Dehaan, R.L., 2019. Modeling mid-season rice nitrogen uptake using multispectral satellite data. Remote Sens. 11, 1837. https://doi.org/10.3390/rs11151837.

Busetto, L., Casteleyn, S., Granell, C., Pepe, M., Barbieri, M., Campos-Taberner, M., Casa, R., Collivignarelli, F., Confalonieri, R., Crema, A., Garcia-Haro, F.J., Gatti, L., Gitas, I.Z., Gonzalez-Perez, A., Grau-Muedra, G., Guarneri, T., Holecz, F., Katsantonis, D., Minakou, C., Miralles, I., Movedi, E., Nutini, F., Pagani, V., Palombo, A., Paola, F.D., Pascucci, S., Pignatti, S., Rampini, A., Ranghetti, L., Ricciardelli, E., Romano, F., Stavrakoudis, D.G., Stroppiana, D., Viggiano, M., Boschetti, M., 2017. Downstream services for rice crop monitoring in Europe: from regional to local scale. IEEE J. Sel. Top. Appl. Earth Obs. Remote Sens. 10, 5423–5441. https://doi.org/10.1109/JSTARS.2017.2679159.

Carrijo, D.R., Lundy, M.E., Linquist, B.A., 2017. Rice yields and water use under alternate wetting and drying irrigation: a meta-analysis. Field Crops Res. 203, 173–180. https://doi.org/10.1016/j.fcr.2016.12.002.

Chauhan, B.S., Jabran, K., Mahajan, G. (Eds.), 2017. Rice Production Worldwide, Springer International Publishing, Cham, Switzerland, 247.

Darbyshire, R., Crean, E., Dunn, T., Dunn, B., 2019. Predicting panicle initiation timing in rice grown using water efficient systems. Field Crops Res. 239, 159–164. https://doi.org/10.1016/j.fcr.2019.05.018.

Dunn, B.W., Dunn, T.S., Beecher, H.G., Dunn, B.W., Dunn, T.S., Beecher, H.G., 2014. Nitrogen timing and rate effects on growth and grain yield of delayed permanent-water rice in south-eastern Australia. Crop Pasture Sci. 65, 878–887. https://doi.org/10.1071/CP13412.

Dunn, B.W., Gaydon, D.S., 2011. Rice growth, yield and water productivity responses to irrigation scheduling prior to the delayed application of continuous flooding in south-east Australia. Agric. Water Manag. 98, 1799–1807. https://doi.org/10.1016/j.agwat.2011.07.004.

Fisher, A., Flood, N., Danaher, T., 2016. Comparing Landsat water index methods for automated water classification in eastern Australia. Remote Sens. Environ. 175, 167–182. https://doi.org/10.1016/j.rse.2015.12.055.

Frantz, D., 2019. FORCE-Landsat. sentinel-2 analysis ready data and beyond. Remote Sens. 11, 1124. https://doi.org/10.3390/rs11091124.

Gao, B.c., 1996. NDWI-A normalized difference water index for remote sensing of vegetation liquid water from space. Remote Sens. Environ. 58, 257–266. https://doi.org/10.1016/S0034-4257(96)00067-3.

Gorelick, N., Hancher, M., Dixon, M., Ilyushchenko, S., Thau, D., Moore, R., 2017. Google earth engine: planetary-scale geospatial analysis for everyone. Remote Sens. Environ. 202, 18–27. https://doi.org/10.1016/j.rse.2017.06.031.

Guo, Y., Jia, X., Paull, D., Benediktsson, J.A., 2019. Nomination-favoured opinion pool for optical-SAR-synergistic rice mapping in face of weakened flooding signals. ISPRS J. Photogramm. Remote Sens. 155, 187–205. https://doi.org/10.1016/j.isprsjprs.2019.07.008.

Herring, M.W., Robinson, W.A., Zander, K.K., Garnett, S.T., 2021. Increasing water-use efficiency in rice fields threatens an endangered waterbird. Agric., Ecosyst. Environ. 322, 107638 https://doi.org/10.1016/j.agee.2021.107638.

Houborg, R., McCabe, M.F., 2018a. A cubesat enabled spatio-temporal enhancement method (CESTEM) utilizing planet, Landsat and MODIS data. Remote Sens. Environ. 209, 211–226. https://doi.org/10.1016/j.rse.2018.02.067.

Houborg, R., McCabe, M.F., 2018b. Daily retrieval of NDVI and LAI at 3 m resolution via the fusion of CubeSat, Landsat, and MODIS data. Remote Sens. 10, 890. https://doi.org/10.3390/rs10060890.

Humphreys, E., Lewin, L.G., Khan, S., Beecher, H.G., Lacy, J.M., Thompson, J.A., Batten, G.D., Brown, A., Russell, C.A., Christen, E.W., Dunn, B.W., 2006. Integration of approaches to increasing water use efficiency in rice-based systems in southeast Australia. Field Crops Res. 97, 19–33. https://doi.org/10.1016/j.fcr.2005.08.020.

Inoue, Y., Sakaiya, E., Wang, C., 2014. Capability of C-band backscattering coefficients from high-resolution satellite SAR sensors to assess biophysical variables in paddy rice. Remote Sens. Environ. 140, 257–266. https://doi.org/10.1016/j.rse.2013.09.001.

Ji, L., Zhang, L., Wylie, B., 2009. Analysis of dynamic thresholds for the normalized difference water index. Photogramm. Eng. Remote Sens. 75, 1307–1317. https://doi.org/10.14358/PERS.75.11.1307.

Li, J., Roy, D.P., 2017. A global analysis of Sentinel-2A, Sentinel-2B and Landsat-8 data revisit intervals and implications for terrestrial monitoring. Remote Sens. 9, 902. https://doi.org/10.3390/rs9090902.

Lin, L.I.K., 1989. A concordance correlation coefficient to evaluate reproducibility. Biometrics 45, 255–268. https://doi.org/10.2307/2532051.

Linquist, B.A., Anders, M.M., Adviento-Borbe, M.A.A., Chaney, R.L., Nalley, L.L., daRosa, E.F., van Kessel, C., 2015. Reducing greenhouse gas emissions, water use,

and grain arsenic levels in rice systems. Glob. Change Biol. 21, 407–417. https://doi.org/10.1111/gcb.12701.

Myers, E., Kerekes, J., Daughtry, C., Russ, A., 2019. Assessing the impact of satellite revisit rate on estimation of corn phenological transition timing through shape model fitting. Remote Sens. 11, 2558. https://doi.org/10.3390/rs11212558.

Nelson, A., Setiyono, T., Rala, A.B., Quicho, E.D., Raviz, J.V., Abonete, P.J., Maunahan, A.A., Garcia, C.A., Bhatti, H.Z.M., Villano, L.S., Thongbai, P., Holecz, F., Barbieri, M., Collivignarelli, F., Gatti, L., Quilang, E.J.P., Mabalay, M.R.O., Mabalot, P.E., Barroga, M.I., Bacong, A.P., Detoito, N.T., Berja, G.B., Varquez, F., Wahyunto, Kuntjoro, D., Murdiyati, S.R., Pazhanivelan, S., Kannan, P., Mary, P.C.N., Subramanian, E., Rakwatin, P., Intrman, A., Setapayak, T., Lertna, S., Minh, V.Q., Tuan, V.Q., Duong, T.H., Quyen, N.H., Van Kham, D., Hin, S., Veasna, T., Yadav, M., Chin, C., Ninh, N.H., 2014. Towards an operational SAR-based rice monitoring system in Asia: examples from 13 demonstration sites across Asia in the RIICE project. Remote Sens. 6, 10773–10812. https://doi.org/10.3390/rs61110773.

Ni, R., Tian, J., Li, X., Yin, D., Li, J., Gong, H., Zhang, J., Zhu, L., Wu, D., 2021. An enhanced pixel-based phenological feature for accurate paddy rice mapping with Sentinel-2 imagery in Google Earth Engine. ISPRS J. Photogramm. Remote Sens. 178, 282–296. https://doi.org/10.1016/j.isprsjprs.2021.06.018.

Nie, L., Peng, S., Chen, M., Shah, F., Huang, J., Cui, K., Xiang, J., 2012. Aerobic rice for water-saving agriculture. A review. Agron. Sustain. Dev. 32, 411–418. https://doi.org/10.1007/s13593-011-0055-8.

Niel, T.G.V., McVicar, T.R., 2003. A simple method to improve field-level rice identification: toward operational monitoring with satellite remote sensing. Aust. J. Exp. Agric. 43, 379. https://doi.org/10.1071/EA02182.

Nieto, L., Houborg, R., Zajdband, A., Jumpasut, A., Prasad, P.V.V., Olson, B.J.S.C., Ciampitti, I.A., 2022. Impact of high-cadence earth observation in maize crop phenology classification. Remote Sens. 14, 469. https://doi.org/10.3390/rs14030469.

Pedregosa, F., Varoquaux, G., Gramfort, A., Michel, V., Thirion, B., Grisel, O., Blondel, M., Prettenhofer, P., Weiss, R., Dubourg, V., Vanderplas, J., Passos, A., Cournapeau, D., Brucher, M., Perrot, M., Duchesnay, E., 2011. Scikit-learn: machine learning in python. J. Mach. Learn. Res. 12, 2825–2830.

Planet Fusion Team, 2021. Planet Fusion Monitoring Technical Specification, Version 1.0.0-beta.3, San Francisco, CA. ⟨https://assets.planet.com/docs/Planet_fusion_specification_March_2021.pdf⟩. (Accessed19 October 2021).

Qiu, R., Katul, G.G., Wang, J., Xu, J., Kang, S., Liu, C., Zhang, B., Li, L., Cajucom, E.P., 2021. Differential response of rice evapotranspiration to varying patterns of warming. Agric. For. Meteorol. 298–299, 108293 https://doi.org/10.1016/j.agrformet.2020.108293.

Ranghetti, L., Boschetti, M., 2022. Updated trends of water management practice in the Italian rice paddies from remotely sensed imagery. Eur. J. Remote Sens. 55, 1–9. https://doi.org/10.1080/22797254.2021.2002726.

Ranghetti, L., Cardarelli, E., Boschetti, M., Busetto, L., Fasola, M., 2018. Assessment of water management changes in the Italian rice paddies from 2000 to 2016 using satellite data: a contribution to agro-ecological studies. Remote Sens. 10, 416. https://doi.org/10.3390/rs10030416.

Sadeh, Y., Zhu, X., Chenu, K., Dunkerley, D., 2019. Sowing date detection at the field scale using CubeSats remote sensing. Comput. Electron. Agric. 157, 568–580. https://doi.org/10.1016/j.compag.2019.01.042.

Skakun, S., Wevers, J., Brockmann, C., Doxani, G., Aleksandrov, M., Batic, M., Frantz, D., Gascon, F., Gómez-Chova, L., Hagolle, O., López-Puigdollers, D., Louis, J., Lubej, M., Mateo-García, G., Osman, J., Peressutti, D., Pflug, B., Puc, J., Richter, R., Roger, J.C., Scaramuzza, P., Vermote, E., Vesel, N., Zupanc, A., Žust, L., 2022. Cloud mask intercomparison eXercise (CMIX): an evaluation of cloud masking algorithms for Landsat 8 and Sentinel-2. Remote Sens. Environ. 274, 112990 https://doi.org/10.1016/j.rse.2022.112990.

Stroppiana, D., Boschetti, M., Azar, R., Barbieri, M., Collivignarelli, F., Gatti, L., Fontanelli, G., Busetto, L., Holecz, F., 2019. In-season early mapping of rice area and flooding dynamics from optical and SAR satellite data. Eur. J. Remote Sens. 52, 206–220. https://doi.org/10.1080/22797254.2019.1581583.

Thorp, K.R., Drajat, D., 2021. Deep machine learning with Sentinel satellite data to map paddy rice production stages across West Java, Indonesia. Remote Sens. Environ. 265, 112679 https://doi.org/10.1016/j.rse.2021.112679.

Torbick, N., Chowdhury, D., Salas, W., Qi, J., 2017. Monitoring rice agriculture across myanmar using time series Sentinel-1 assisted by Landsat-8 and PALSAR-2. Remote Sens. 9, 119. https://doi.org/10.3390/rs9020119.

Waldner, F., Chen, Y., Lawes, R., Hochman, Z., 2019. Needle in a haystack: mapping rare and infrequent crops using satellite imagery and data balancing methods. Remote Sens. Environ. 233, 111375 https://doi.org/10.1016/j.rse.2019.111375.

Ward, R., Brickhill, H., Bull, N., Dunn, B., Dunn, T., Fowler, J., Hart, J., Mauger, T., 2021. Rice Growing Guide 2021. ⟨https://www.dpi.nsw.gov.au/_data/assets/pdf_file/0004/1361173/RGG-2021-web-final-26Oct2021.pdf⟩. (Accessed 28 July 2022).

Wolski, P., Murray-Hudson, M., Thito, K., Cassidy, L., 2017. Keeping it simple: monitoring flood extent in large data-poor wetlands using MODIS SWIR data. Int. J. Appl. Earth Obs. Geoinf. 57, 224–234. https://doi.org/10.1016/j.jag.2017.01.005.

Wolters, S., Söderström, M., Piikki, K., Reese, H., Stenberg, M., 2021. Upscaling proximal sensor N-uptake predictions in winter wheat (Triticum aestivum L.) with Sentinel-2 satellite data for use in a decision support system. Precis. Agric. 22, 1263–1283. https://doi.org/10.1007/s11119-020-09783-.

Xiao, D., Niu, H., Guo, F., Zhao, S., Fan, L., 2022. Monitoring irrigation dynamics in paddy fields using spatiotemporal fusion of Sentinel-2 and MODIS. Agric. Water Manag. 263, 107409 https://doi.org/10.1016/j.agwat.2021.107409.